Enhancement of Dielectric Permittivity of $Ti_3C_2T_x$ Mxene/Polymer Composites by Controlling Flake Size and Surface Termination

Shaobo Tu[+], Qiu Jiang[+], Junwei Zhang, Xin He, Mohamed Nejib Hedhili, Xixiang Zhang and Husam N. Alshareef**

Materials Science and Engineering, Physical Science and Engineering Division, King Abdullah University of Science and Technology (KAUST), Thuwal 23955-6900, Saudi Arabia

[+]*Contribute equally to the work*

E-mail: xixiang.zhang@kaust.edu.sa, husam.alshareef@kaust.edu.sa

KEYWORDS: MXene flakes, size engineering, surface terminations, dielectric permittivity, microscopic dipole

ABSTRACT

We report a strong effect of MXene flake size and surface termination on the dielectric permittivity of MXene polymer composites. Specifically, poly(vinylidene fluoride-trifluoro-ethylene-chlorofluoroehylene) or P(VDF-TrFE-CFE) polymer embedded with large (ca. 4.5 μm) $Ti_3C_2T_x$ flakes reaches a dielectric permittivity as high as 10^5 near the percolation limit of 15.3 wt % MXene loading. In comparison, the dielectric permittivity of MXene/P(VDF-TrFE-CFE) using small (ca. 1.5 μm) $Ti_3C_2T_x$ flakes (S-MXene) reaches a dielectric permittivity of 10^4 near the percolation limit of 16.8 wt%. Meanwhile, increasing the concentration of surface functional groups on MXene surface (-O, -F, -OH) by extending the etching time, gives a dielectric constant of 2204 near the percolation limit of 15.7 wt%. The ratio of permittivity to loss factor of our large flake composite is superior to that of small flake composite, and to all previously reported carbon-based fillers in P(VDF-TrFE-CFE). We show that the dielectric permittivity enhancement is strongly related to the charge accumulation at the surfaces between the two dimensional (2D) MXene flakes and the polymer matrix under external applied electric field.

1. INTRODUCTIONS

Nanocomposites with conducting, semiconducting, and insulating fillers dispersed in Poly(vinylidene fluoride) (PVDF)-based polymers have recently triggered renewed interest thanks to their potential in various electronic applications, including flexible electronics, energy harvesters, charge storage capacitors, and strain sensors.[1-6] In a previous report,[7] we investigated the dielectric constant enhancement of P(VDF-TrFE-CFE) using $Ti_3C_2T_x$ MXene flakes as conducting filler. The MXene/P(VDF-TrFE-CFE) composite resulted in a dielectric permittivity over 100,000 near the percolation limit, which was the highest dielectric constant reported for P(VDF-TrFE-CFE)-based composites.[8-12] Furthermore, MXene/P(VDF-TrFE-CFE) composite may have a promising application in flexible electronics, fractional-order capacitors, and triboelectric generators.

MXenes, a new family of 2D transition metal carbides, nitrides, and carbonitrides with the general formula of $M_{n+1}X_nT_x$, have recently raised considerable attention due to their promising characteristics in various applications, including energy storage, flexible electronics, water purifications, nanofiltration, photocatalysis, and biosensors.[13-20] In $M_{n+1}X_nT_x$, M is an early transition metal, X is carbon and/or nitrogen, T_x represents the surface functional groups (e.g. OH, O, and/or F groups), and n = 1, 2, or 3. For two dimensional materials, including graphene oxide (GO),[21] carbon nanotube (CNT),[22] and boron nitride (BN),[23] the aspect ratio and surface chemistry are critical to the electrical and mechanical properties of their nanocomposites. However, there have been no relevant reports on the size and surface chemistry effect of MXene nanosheets on the dielectric properties of MXene/polymer nanocomposites.

In this study, we show that both flake size and concentration of surface terminations are effective methods for improving the dielectric properties of MXene-polymer composites.

2. EXPERIMENTAL SECTION

2.1 Preparation of MXene. The synthesis of few-layered $Ti_3C_2T_x$ was prepared following a previous report.[30] Briefly, 1g of Ti_3AlC_2 powder (Carbon-Ukraine ltd. particle size < 40 μm) was slowly added to the etchant solution, which was prepared by adding 2g LiF to 40 mL 9M HCl. The mixture was stirred for 10 mins and then was transferred to an oil bath. The temperature of the oil bath was kept at 35 °C and the mixture was stirred in oil bath for 24 hour. After etching, the suspension was washed with deionized water until PH reached > 6. Next, the sediment was again mixed with deionized water and sonicated in ice bath for different times ranging from 30 mins to 3 hours to get few-layer $Ti_3C_2T_x$ with different flake sizes. The sonication process was carried out under N_2 bubbling. After sonication, the suspension was centrifuged for 10 mins at 3500 rpm, the resultant supernatant with dark green color was collected and bubbled with N_2 for future applications. The concentration of the $Ti_3C_2T_x$ solution was measured by filtering specific amounts of colloidal solution through a polypropylene filter (3,501 coated PP, Celgard LLC, Charlotte, NC), followed by overnight drying under a vacuum at 70 °C. Higher concentration of –F, -O, and –OH surface terminations were formed on MXene surface after continuous etching for 96 h.

2.2 Fabrication of Nanocomposites. The previously collected $Ti_3C_2T_x$ MXene resultant supernatant was centrifuged for 10 mins at 6000 rpm, and the precipitation of MXene was collected and suspended in 3 ml dimethylformamide (DMF) *via* shaking for one hour. According to intended MXene loadings, the desired quantity of P(VDF-TrFE-CFE) (61.5/30.2/8.3 mol% Piezotech S.A., France) was dissolved into the suspensions under continuous stirring for 30 minutes at 80 °C. After two hour's gentle ultrasonication, the MXene/P(VDF-TrFE-CFE) suspension was directly cast onto platinum-coated silicon substrates. The composites were then dried overnight in a nitrogen-protected glove box and were finally annealed at 70 °C in a vacuum oven for two days. Subsequently, top Ti (100

nm)/Au (50 nm) electrodes were deposited on the films (with an average thickness of 100 um) by electron-beam evaporation through a shadow mask for dielectric characterization.

2.3 Equipment and Characterization. The weight percent of MXene in the polymer matrix was confirmed by thermogravimetric analysis. In addition, the structure and properties of MXene-polymer composites were investigated by using XRD (Bruker D2 Phaser) and FT-IR in transmission mode (Nicolet iS10, Thermo Scientific). Raman spectroscopy was performed on a Horiba Aramis Raman Microscope with 633-nm laser excitation. The MXene sheets were investigated with TEM (Titan Cs Image), SEM (Nova Nano), AFM (Asylum research), and XPS (Amicus). Surface and cross-sectional images of composite films were observed with TEM (Titan Cs Image). Frequency-dependent capacitance was measured with an Agilent LCR meter (4980A) in the frequency range of 1K Hz to 100 KHz and an oscillation signal of ~50 mV_{rms} with a parallel equivalent circuit. The current density vs electric field (J-E) loops in our manuscript were derived from I-V curves measured using an Agilent B1500A system. The J-E loops were measured by using a direct current (DC) source with a field ramping rate of 50 V cm^{-1} s^{-1}. The dwell time was 0.5 s for each step.

3. RESULTS AND DISCUSSION

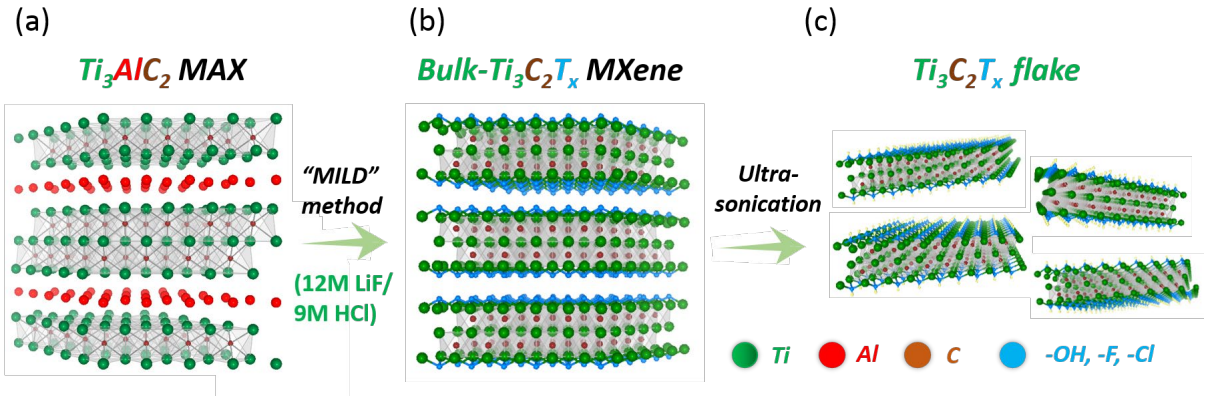

Figure 1. Schematic illustrating the structure of (a) Ti_3AlC_2 MAX phase, (b) bulk-$Ti_3C_2T_x$ MXene after etching and delamination, (c) MXene two dimensional (2D) flakes of different sizes obtained by ultra-sonication.

Figure 1 illustrates the synthesis process used to prepare MXene flakes. (see Methods for the detailed process). Bulk-$Ti_3C_2T_x$ MXene was first prepared from $Ti_3C_2T_x$ bulk MAX phase using the "MILD" method which involves using LiF and HCl for etching and delamination.[24] MXene 2D flakes with different sizes were obtained by changing ultra-sonication time of the bulk $Ti_3C_2T_x$. After 1 hour sonication, we obtained a flake size of 4-5 μm, which are henceforth denoted as large MXene flakes (L-MXene). After 3 hour sonication, we obtained a flake size of 1-2 μm, which are henceforth denoted as small MXene flakes (S-MXene). The MXene flakes obtained by sequential 96 h etching and 1 hour sonication are denoted as termination-rich large MXene flakes (TL-MXene). The L-MXene/P(VDF-TrFE-CFE), S-MXene/P(VDF-TrFE-CFE), and TL-MXene/P(VDF-TrFE-CFE) composites were prepared by dispersing the L-MXene, S-MXene, and TL-MXene in the P(VDF-TrFE-CFE)/Dimethylformamide (DMF) solution, respectively, followed by casting on platinum-coated silicon substrate, drying overnight in glovebox and finally annealing in vacuum oven at 70°C for 48 hours. A film with an average thickness of 100 μm was obtained, as measured by a Profilometer, and the corresponding weight percent of MXene in the composite was confirmed by thermogravimetric analysis (TGA) (Figure S1). Subsequently, Ti/Au contacts were deposited on the top of the MXene-polymer films through a shadow mask by e-beam evaporation.

The high resolution transmission electron microscopy (HRTEM) image in Figure 2a shows the typical morphology of single-layered MXene flake that has been prepared through a sequence of etching and delamination processes discussed earlier. Inset (i) shows the lattice resolved HRTEM image of the MXene sheets which indicates that Ti atoms form a hexagonal lattice. Inset (ii) depicts the selected area electron diffraction (SAED) pattern of the $Ti_3C_2T_x$ MXene sheets in Fig. 2a obtained from the [001] direction, which confirms the hexagonal symmetry of the Ti sublattice. The marked reciprocal vectors represent their corresponding

Miller indices of the planes in the real lattice. Furthermore, Figure 2b illustrates the scanning transmission electron microscopy (STEM) image of the $Ti_3C_2T_x$ MXene, and its corresponding elemental mapping, which shows a uniform distribution of Ti, C, F and O elements in the MXene sheets.

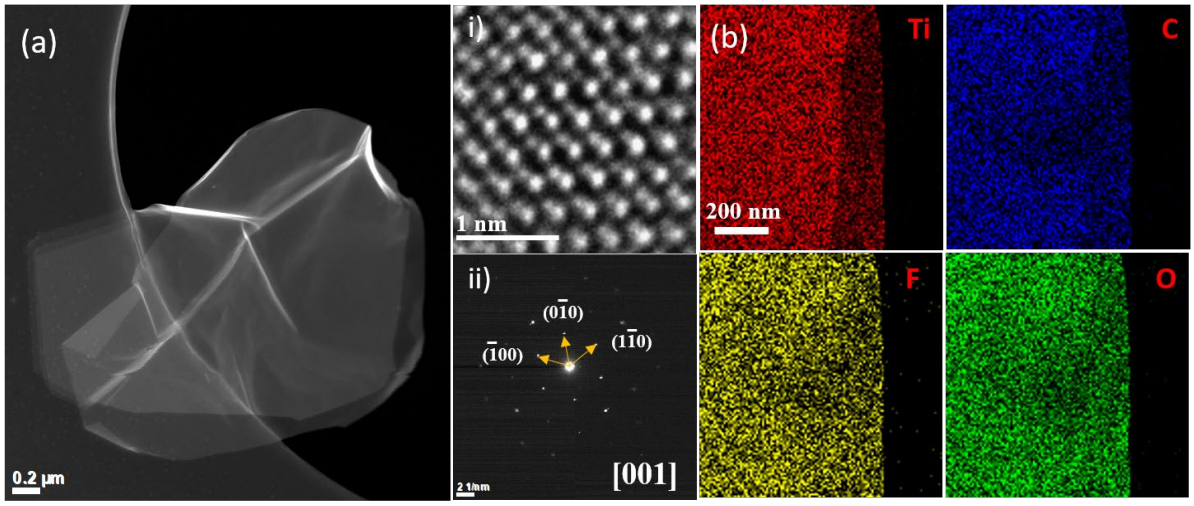

Figure 2. HRTEM image of (a) $Ti_3C_2T_x$ MXene flakes; Inset i: Lattice resolved HRTEM image of $Ti_3C_2T_x$ which shows the Ti atom hexagonal lattice. Inset ii: SAED pattern of the $Ti_3C_2T_x$ MXene flake taken along the [001] axis. (b) Scanning transmission electron microscopy (STEM) image of the $Ti_3C_2T_x$ MXene, and its corresponding elemental mapping.

Figure 3a shows the atomic force microscopy (AFM) image of L-MXene flakes with a 5.0 µm lateral size. Figure 3b shows the AFM image of overlapping S-MXene sheets with a 1.5 µm lateral size. Figure 3c and d illustrate the size distribution of L-MXene and S-MXene, which reveal that the average lateral size of L-MXene and S-MXene is 4.5 µm and 1.5 µm, respectively. The cross-sectional SEM image of MXene/P(VDF-TrFE-CFE) shown in Figure S2a reveals that the MXene flakes dispersed inside polymer matrix without aggregation, which was further confirmed by AFM image of the same composite (Figure S2b). Both the Raman spectrum and Fourier-transform infrared spectroscopy (FIIR) of $Ti_3C_2T_x$ MXene flakes and MXene/polymer composites suggest that there are no vibrational changes during

the mixing process (Figure S2c-d). The cross-sectional SEM image of S-MXene/P(VDF-TrFE-CFE) and TL-MXene/P(VDF)-TrFE-CFE) composite are shown in Figure S3.

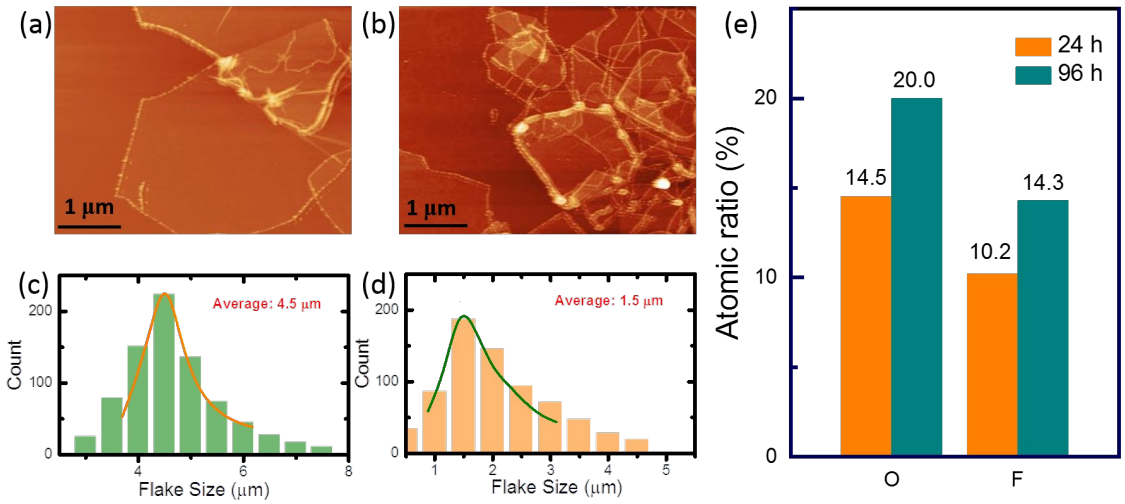

Figure 3. (a) AFM images of large-sized $Ti_3C_2T_x$ MXene (L-MXene) flakes deposited on mica. (b) AFM images of small-sized $Ti_3C_2T_x$ MXene (S-MXene) flakes. (c) Statistical distribution of L-MXene flake size. (d) Statistical distribution of S-MXene flake size. e) The concentration of surface termination on MXene sheets after 24 h and 96 h etching, measured using X-ray photoelectron spectroscopy.

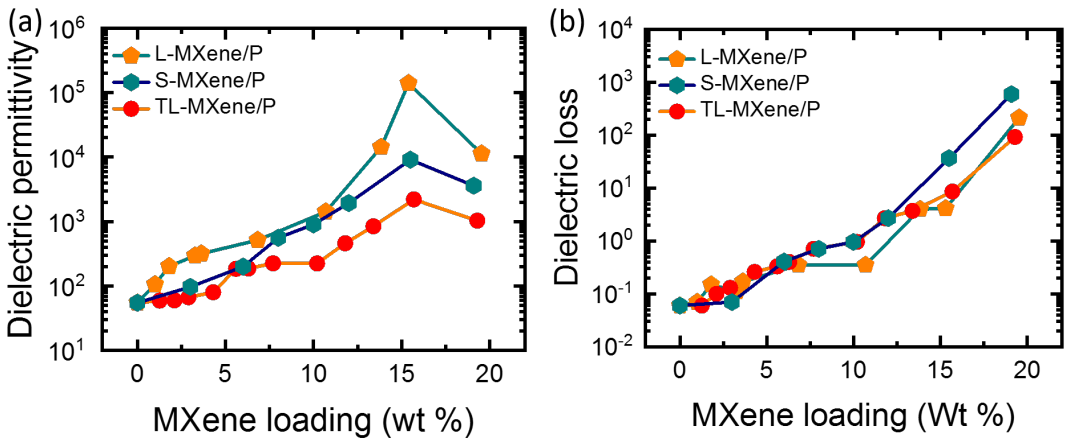

Figure 4. (a) Dielectric permittivity and (b) dielectric loss of the L-MXene/P(VDF-TrFE-CFE), S-MXene/P(VDF-TrFE-CFE), and TL-MXene/P(VDF-TrFE-CFE) composites versus MXene loading measured at room temperature and 1kHz.

Additionally, X-ray photoelectron spectroscopy (XPS) was used to characterize the surface chemistry of MXene sheets after 24 h and 96 h etching. The analysis reveals the presence of –OH, -O, and –F functional groups on the $Ti_3C_2T_x$ MXene surface (Figure S4). Compared with 24 h etching, the percentage of O (-O, -OH) and F increase from 14.5 and

10.2 to 20.0 and 14.3, respectively. These results indicate the oxidation of MXene flakes during the over-etching process, from which we can conclude that the surface of MXene flakes after 96 h etching is rich in -F, -O, and -OH (Figure 3e).

Figure 4a displays the dielectric permittivity of L-MXene/P(VDF-TrFE-CFE), S-MXene/P(VDF-TrFE-CFE), and TL-MXene/P(VDF-TrFE-CFE) composites as a function of filler loading, which indicate that the dielectric permittivity of these composites initially increases with MXene filler concentration. A dielectric constant > 100,000 was reached in case of the composite with 15.3 wt % L-MXene in terpolymer; in comparison, a dielectric constant of 10,000 was reached in case of the S-MXene/polymer composite with a 16.8 wt % S-MXene loading; the dielectric constant of TL-MXene/terpolymer composite reached 2204 near the percolation limit at around 16.0 wt%. The obvious degradation of dielectric permittivity of TL-MXene/P(VDF-TrFE-CFE) composites can probably be ascribed to the high dense concentration of negative surface functional groups on the TL-MXene surface, which could effectively decrease charge accumulation on the TL-MXene/polymer interface under the externally-applied electric field. In all these cases, further increases in MXene loading leads to a drop in the dielectric constant value, which indicates that we have reached the percolation limit for all the L-MXene/P(VDF-TrFE-CFE), S-MXene/P(VDF-TrFE-CFE), and TL-MXene/P(VDF-TrFE-CFE) composites at 15-17 wt% MXene loading. The dielectric permittivity for composites that contain conductive fillers embedded in an insulating polymer matrix follows the power law according to percolation theory.[25-29]

$$\varepsilon_{eff} \propto \varepsilon_m(\varphi_c - \varphi_p)^{-q} \text{ for } \varphi_p < \varphi_c, \quad (1)$$

where ε_m is the dielectric constant of the insulation matrix, φ_p is the volume fraction of metallic fillers, φ_c is the volume fraction at percolation threshold, and q is the critical exponent.

Figure 4b additionally present the dielectric loss of L-MXene/P(VDF-TrFE-CFE) and S-MXene/P(VDF-TrFE-CFE) composites. Up to 10 wt % MXene loading, the dielectric constant and loss factor of L-MXene/polymer composite increase 25 times (from 55 to 1425) and 5 times (from 0.06 to 0.35), respectively. Over the same range of MXene loading (up to 10 wt%), the dielectric constant and loss factor of S-MXene/polymer composite increases 10 times (from 55 to 560) and 9 times (from 0.06 to 0.61), and those of TL-MXene/polymer composite increases 4 times (from 55 to 225) and 10 times (from 0.06 to 0.65). It is clear that the dielectric constant is more significantly enhanced, at a fixed MXene loading, when the composite uses L-MXene. Figure S5 and Table S1 in Supporting Information specify the dielectric constant and dielectric loss of L-MXene/P(VDF-TrFE-CFE), S-MXene/P(VDF-TrFE-CFE) and TL- MXene/P(VDF-TrFE-CFE) composites at all the MXene loadings prepared in this study.

To obtain an insight into the cause of the different levels of dielectric constant enhancement by changing MXene flake size, we performed unipolar measurements on both L-MXene/P(VDF-TrFE-CFE) and S-MXene/P(VDF-TrFE-CFE) composites with 8.0 wt % MXene loading (see Methods for process details). Before these measurements, the composites had been poled using negative 2.5 kV cm^{-1} for five minutes at room temperature. Figure 5a-c show the unipolar J-E curves of L-MXene/polymer, S-MXene/polymer and TL-MXene composites with the same 8.0 wt% MXene loading, respectively. The unipolar J-E curves (0 $\rightarrow$ 2.5 kV cm^{-1}) exhibit a bump at about 1.5 kV cm^{-1} in the first cycle, which must be due to the current induced by some dipole reversal since the sample was previously poled by a negative voltage. After most "dipoles" had been aligned in the positive direction during the first positive electric field application, no bump was observed in either the increasing-field or decreasing-field curve in the following J-E loops (3rd to 19th). The leakage-corrected polarization can be calculated as follows:

$$P(t) = \int_0^t [J(t) - J_d(t)]dt \,, \qquad (2)$$

where *J(t)* is the measured total current density, including the current induced by dipole reversal and leakage, and $J_d(t)$ is the measured current density after several cycles of electric field, which approximately represents the leakage current.

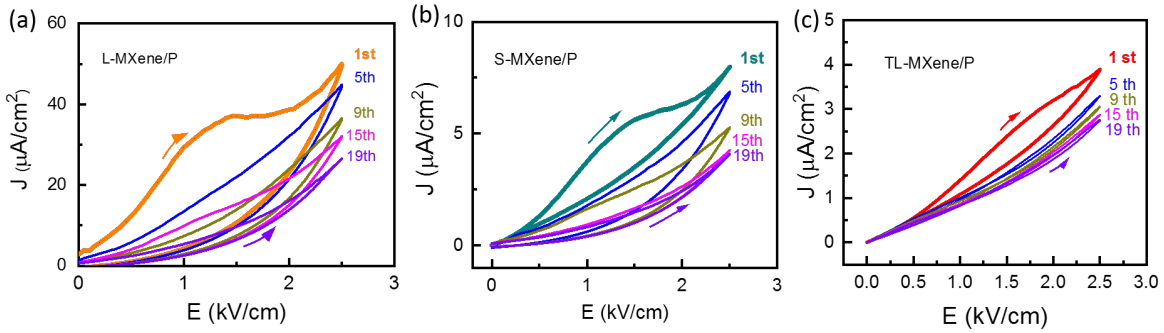

Figure 5. (a-c) Unipolar J−E loops measured with a positive field applied to the L-MXene/P(VDF-TrFE-CFE), S-MXene/P(VDF-TrFE-CFE), and TL-MXene/P(VDF-TrFE-CFE) composite (8.0 wt % MXene), which have been prepoled with a negative field of 2.5 kV cm^{-1}.

The leakage-corrected current and the derived remnant polarization of L-MXene/P(VDF-TrFE-CFE) composite with 8.0wt % MXene loading are 22.0 μA/cm^2 and 14.0 μC/cm^2, while those of S-MXene/P(VDF-TrfE-CFE) composite with the same MXene loading are 4.1 μA/cm^2 and 4.0 μC/cm^2, and those of TL-MXene/P(VDF-TrFE-CFE) with the same MXene loading are 1.9 μA/cm^2 and 0.8 μC/cm^2, respectively. This result clearly indicates that the accumulated charges at the L-MXene/polymer interface (which form the switchable dipole) are larger than that of S-MXene/polymer composite and TL-MXene/polymer composites, which means that the effective dielectric permittivity of L-MXene/polymer composite is higher than that of S-MXene/polymer composite and TL-MXene/polymer with the same MXene loading.

4. CONCLUSIONS

We have developed a method to enhance the dielectric constant of MXene/P(VDF-TrFE-CFE) composites by engineering the flake size and concentration of surface functional groups. The MXene/P(VDF-TrFE-CFE) composite using large (4.5 μm) MXene flakes reaches a dielectric permittivity as high as 10^5 near the percolation limit. In comparison, the MXene/P(VDF-TrFE-CFE) composite using small MXene flakes reaches a dielectric permittivity of 10^4 near the percolation limit, while the dielectric constant of TL-MXene/P(VDF-TrFE-CFE) composite reaches to 2204 near the percolation limit of 16.0 wt%. These results were explained based on the accumulation of charges at the interfaces between the two dimensional (2D) MXene flakes and the polymer matrix, where the switchable microscopic dipoles are situated.

ASSOCIATED CONTENT

Supporting Information

Figure S1. Thermogravimetric analysis of a) L-MXene/P(VDF-TrFE-CFE) b) S-MXene/P(VDF-TrFE-CFE) composites c) TL-MXene/P(VDF-TrFE-CFE) composites.

Figure S2. a) A cross-sectional SEM image of MXene/P(VDF-TrFE-CFE) composite. b) An AFM image of MXene/P(VDF-TrFE-CFE) composite. c) Raman spectra and d) FT-IR of MXene/P(VDF-TrFE-CFE) composites.

Figure S3. A cross-sectional SEM image of a) S-MXene/P(VDF-TrFE-CFE) composite. b) TL-MXene/P(VDF-TrFE-CFE) composite.

Figure S4. X-ray photoelectron spectroscopy spectra of $Ti_3C_2T_x$ MXene etched for a) 24 h and b) 96 h.

Figure S5. Dielectric constant of a) L-MXene/P(VDF-TrFE-CFE) composites, b) S-MXene/P(VDF-TrFE-CFE) composites, c) TL-MXene/P(VDF-TrFE-CFE) composites.

Dielectric loss of d) L-MXene/P(VDF-TrFE-CFE) composites, e) S-MXene/P(VDF-TrFE-CFE) composites, f) TL-MXene/P(VDF-TrFE-CFE) composites.

Table S1. Dielectric permittivity and dielectric loss of L-MXene/P(VDF-TrFE-CFE), S-MXene/P(VDF-TrFE-CFE), and TL-MXene/P(VDF-TrFE-CFE) composites with different MXene loadings.

The Supporting Information is available free of charge on the ACS Publications Websites at http://pubs.acs.org.

ACKNOLEDGEMENTS

Research reported in this publication is supported by King Abdullah University of Science and Technology (KAUST). The TEM analysis was individually completed by Dr. Junwei Zhang. The authors would like to thank Chenhui Zhang and Dr. Fei Xue for their helpful discussion, and the Advanced Nanofabrication, Imaging and Characterization Laboratory at KAUST for their excellent assistance.

REFERENCES

(1) Dang, Z. M.; Wang, L.; Wang, H. Y.; Nan, C. W.; Xie, D.; Yin, Y.; Tjong, S. C., Giant Dielectric Permittivities in Functionalized Carbon-Nanotube/Electroactive-Polymer Nanocomposites. *Adv. Mater.***2007***,19,* 852–857.

(2) Dang, Z.M.; Wang, L.; Wang, H.Y.; Nan, C.W.; Xie, D.; Yin, Y.; Tjong, S. C., Rescaled Temperature Dependence of Dielectric Behavior of Ferroelectric Polymer Composites. *Appl. Phys. Lett.* **2005**, *86*, 172905.

(3) Lee, Y. T.; Kwon, H.; Kim, J. S.; Kim, H. H.; Lee, Y. J.; Lim, J. A.; Song, Y. W.; Yi, Y. J.; Choi, W. K.; Hwang, D. K.; Im, S., Noncolatile Ferroelectric Memory Circuit Using Black Phosphorus Nanosheet-Based Field-Effect Transistors with P(VDF-TrFE) Polymer. *ACS nano* **2015**, *9*, 10394-10401.

(4) Elshurafa, A. M.; Almadhoun, M. N.; Salama, K. N.; Alshareef, H. N., Microscale Electrostatic Fractional Capacitors Using Reduced Graphene Oxide Percolated Polymer Composites. *Appl. Phys. Lett.* **2013**, *102*, 232901.

(5) Yang, Y.; Zhang, H. L.; Zhu, G.; Lee, S. M.; Lin, Z. H.; Wang, Z. L., Flexible Hybrid Energy Cell for Simultaneously Haverting Thermal, Mechanical, and Solar Energies. *ACS nano* **2013**, *7*, 785-790.

(6) Zhang, B.; Zhang, L.; Deng, W.; Jin, L.; Chun, F.; Pan, H.; Gu, B.; Zhang, H.; Lv, Z.; Yang, W.; Wang, Z. L., Self-Powered Acceleratin Sensor Based on Liquid Metal Triboelectric Nanogenerator for Vibration Monitoring. *ACS nano* **2017**, *11*, 7440-7446.

(7) Tu, S. B.; Jiang, Q.; Zhang, X. X.; Alshareef, H. N., Large Dielectric Constant Enhancement in MXene Percolative Polymer Composites. *ACS Nano*, **2018**, *12*, 3369-3377.

(8) Fan, P.; Wang, L.; Yang, J.; Chen, F.; Zhong, M., Graphene/Poly(vinylidene fluoride) Composites with High Dielectric Constant and Low Percolation Threshold. *Nanotechnology* **2012,** *23*, 365702.

(9) Garrett, J. T.; Roland, C. M.; Petchsuk, A.; Chung, T. C., Electrostrictive Behavior of Poly(vinylidene fluoride-trifluoroethylene-chlorotrifluoroethylene). *Appl. Phys. Lett.* **2003,** *83*, 1190-1192.

(10) Han, K.; Li, Q.; Chen, Z.; Gadinski, M. R.; Dong, L.; Xiong, C.; Wang, Q., Suppression of Energy Dissipation and Enhancement of Breakdown Strength in Ferroelectric Polymer–Graphene Percolative Composites. *J. Mater. Chem. C* **2013,** *1*, 7034-7042.

(11) Han, Z.; Li, D.; Wang, X. W.; Zhang, Z. D., Microwave Response of FeCo/Carbon Nanotubes Composites. *J. Appl. Phys.* **2011,** *109*, 07A301.

(12) Almadhoun, M. N.; Hedhili, M. N.; Odeh, I. N.; Xavier, P.; Bhansali, U. S.; Alshareef, H. N., Influence of Stacking Morphology and Edge Nitrogen Doping on the Dielectric Performance of Graphene–Polymer Nanocomposites. *Chem. Mater.* **2014,** *26*, 2856-2861.

(13) Anasori, B.; Lukatskaya, M. R.; Gogotsi, Y., 2D Metal Carbides and Nitrides (MXenes) for Energy Storage. *Nat. Rev. Mater.* **2017,** *2*, 16098.

(14) Lukatskaya, M. R.; Mashtalir, O.; Ren, C. E.; Dall'Agnese, Y.; Rozier, P.; Taberna, P. L.; Naguib, M.; Simon, P.; Barsoum, M. W.; Gogotsi, Y., Cation Intercalation and High Volumetric Capacitance of Two-Dimensional Titanium Carbide. *Science* **2013**, *341*, 1502-1505.

(15) Jiang, Q.; Wu, C.; Wang, Z.; Wang, A. C.; He, J. H.; Wang, Z. L.; Alshareef, H. N. MXene Electrochemical Microsupercapacitor Integrated with Triboelectric Nanogenerator as a Wearable Self-Charging Power Unit. *Nano Energy* **2018**, *45*, 266–272.

(16) Zhang, Q.; Teng, J.; Zou, G.; Peng, Q.; Du, Q.; Jiao, T.; Xiang, J., Efficient Phosphate Sequestration for Water Purification by Unique Sandwich-like MXene/Magnetic Iron Oxide Nanocomposites. *Nanoscale* **2016**, *8*, 7085-7093.

(17) Zou, G.; Guo, J.; Peng, Q.; Zhou, A.; Zhang, Q.; Liu, B., Synthesis of Urchin-like Rutile Titania Carbon Nanocomposites by Iron-facilitated Phase Transformation of MXene for Environmental Remediation. *J. Mater. Chem. A* **2016**, *4*, 489-499.

(18) Wu, X.; Hao, L.; Zhang, J.; Zhang, X.; Wang, J.; Liu, J., Polymer-$Ti_3C_2T_x$ Composite Membranes to Overcome the Trade-off in Solvent Resistant Nanofiltration for Alcohol-based System. *J. Membr. Sci.* 2016**, 515**, 175-188.

(19) Xu, B.; Zhu, M.; Zhang, W.; Zhen, X.; Pei, Z.; Xue, Q.; Zhi, C.; Shi, P., Ultrathin MXene-Micropattern-Based Field-Effect Transistor for Probing Neural Activity. *Adv. Mater.* **2016,** *28*, 3333-3339.

(20) Zhang, X.; Lei, J.; Wu, D.; Zhao, X.; Jing, Y.; Zhou, Z., A Ti-anchored Ti_2CO_2 Monolayer (MXene) as a Single-atom Catalyst for CO Oxidation. *J. Mater. Chem. A* **2016**, *4*, 4871-4876.

(21) Shen, Y.; Zhu, X.; Chen, B., Size Effects of Graphene Oxide Nanosheets on the Construction of Three-dimensional Graphene-based Macrostructures as Adsorbents. *J. Mater. Chem. A* **2016**, *4*, 12106-12118.

(22) Kim, J.; Kim, S. W.; Yun, H.; Kim, B. J., Impact of Size Control of Graphene Oxide Nanosheets for Enhancing Electrical and Mechanical Properties of Carbon Nanotube-polymer Composites. *RSC Adv.* **2017**, *7*, 30221-30228.

(23) Li, Q.; Zhang, G.; Liu, F.; Han, K.; Gadinski, M. R.; Xiong, C.; Wang, Q., Solution-processed Ferroelectric Terpolymer Nanocomposites with High Breakdown Strength and Energy Density Utilizing Boron Nitride Nanosheets. *Energy Environ. Sci.* **2015**, *8*, 922-931.

(24) Naguib, M.; Mashtalir, O.; Carle, J.; Presser, V.; Lu, J.; Hultman, L.; Gogotsi, Y.; Barsoum, M. W., Two-Dimensional Transition Metal Carbides. *ACS nano* **2012**, *6*, 1322-1331.

(25) Nan, C. W.; Shen, Y.; Ma, J., Physical Properties of Composites Near Percolation. *Annu. Rev. Mater. Res.* **2010,** *40*, 131-151.

(26) Prateek; Thakur, V. K.; Gupta, R. K., Recent Progress on Ferroelectric Polymer-Based Nanocomposites for High Energy Density Capacitors: Synthesis, Dielectric Properties, and Future Aspects. *Chem. Rev.* **2016,** *116*, 4260-4317.

(27) Nan, C. W., Physics of Inhomogeneous Inorganic Materials. *Prog. Mater. Sci.* **1993**, *37*, 1-116.

(28) Rahaman, M.; Chaki, T. K.; Khastgir, D., Modeling of DC Conductivity for Ethylene Vinyl Acetate (EVA)/Polyaniline Conductive Composites Prepared through Insitu Polymerization of Aniline in EVA Matrix. *Compos. Sci. Tech.* **2012**, *72*, 1575-1580.

(29) Dang, Z.-M.; Nan, C.-W.; Xie, D.; Zhang, Y.-H.; Tjong, S. C., Dielectric Behavior and Dependence of Percolation Threshold on The Conductivity of Fillers in Polymer-Semiconductor Composites. *Appl. Phys. Lett.* **2004,** *85*, 97-99.

(30) Jiang, Q.; Kurra, N.; Alhabeb, M.; Gogotsi, Y.; Alshareef, H. N., All Pseudocapacitive MXene-RuO_2 Asymmetric Supercapacitors. *Adv. Energy Mater.* **2018**, *8*, 1703043.

TABLE OF CONTENTS GRAPHIC